The Aryl Hydrocarbon Receptor Is Important for Proper Seminiferous Tubule Architecture and Sperm Development in Mice 1

Authors: Hansen, Deborah A., Esakky, Prabagaran, Drury, Andrea, Lamb, Laura, and Moley, Kelle H.

Source: Biology of Reproduction, 90(1)

Published By: Society for the Study of Reproduction

URL: https://doi.org/10.1095/biolreprod.113.108845

BIOLOGY OF REPRODUCTION (2014) **90**(1):8, 1–12
Published online before print 30 October 2013.
DOI 10.1095/biolreprod.113.108845

The Aryl Hydrocarbon Receptor Is Important for Proper Seminiferous Tubule Architecture and Sperm Development in Mice[1]

Deborah A. Hansen,[3] Prabagaran Esakky,[3,4] Andrea Drury,[3,4] Laura Lamb,[4] and Kelle H. Moley[2,4]

[3]*Research, VA St. Louis Health Care System, St. Louis, Missouri*
[4]*Department of Obstetrics and Gynecology, Washington University School of Medicine, St. Louis, Missouri*

ABSTRACT

The aryl hydrocarbon receptor (AHR) is known for its roles in xenobiotic metabolism and essential physiologic processes such as cell growth, death, and differentiation. AHR is also an important regulator of male reproductive processes. However, no studies have characterized the consequences of loss of AHR in spermatogenesis. We used *Ahr* knockout (*Ahr*$^{-/-}$) mice to assess the effects of loss of AHR on the architecture and gene expression of the seminiferous epithelium and functional sperm outcomes. The histopathological defects of the *Ahr*$^{-/-}$ seminiferous epithelium included vacuoles, multinucleated giant cells, hypocellularity with widened intercellular spaces, apical sloughing, and an excess number of retained elongated spermatids. Quantitative real-time PCR revealed significant down-regulation of *Testin* and *Magea4*, indicating Sertoli cell and spermatogenic dysregulation. Moreover, the reduced expression of *Hspa2, Prm1,* and *Prm2* as well as decreased expression of *Nrf2, Sod2,* and *Ucp2* suggested poorly remodeled germ cells with increased vulnerability to oxidative stress. In wild-type sperm, AHR protein was localized to the acrosome and the principal piece of the mature sperm flagellum. The in vitro fertilization rate was significantly lower with *Ahr*$^{-/-}$ sperm as compared to wild-type sperm, and there were morphologic abnormalities of the *Ahr*$^{-/-}$ sperm head and tail. Taken together, our data indicate that AHR plays an important role in normal sperm development.

aryl hydrocarbon receptor, fertilization, Sertoli cell, spermatogenesis

INTRODUCTION

The aryl hydrocarbon receptor (AHR) is a ligand-activated transcription factor that, upon binding to a natural or synthetic compound, translocates to the nucleus, binds to the AHR nuclear transporter (ARNT), and induces expression of many genes [1]. AHR is best known for induction of the cytochrome P450 superfamily of genes (*Cyp1a1* and *Cyp1a2*) and the detoxification of endogenous and exogenous ligands [2, 3].

AHR binds with high affinity and specificity to dioxin-like compounds, which are highly toxic and widely dispersed environmental hazards formed via industrial processes such as incineration and the incomplete combustion of fossil fuels [4, 5]. Exposure to dioxin-like compounds is associated with an array of adverse health effects such as cancers, immune system dysregulation, and endocrine disruption [6, 7]. Additionally, reproductive sequelae of exposure to dioxin-like compounds have been suggested by the prevalence of cardiac defects, cleft palate, renal agenesis, and neural tube defects in the children of male firefighters [8] and veterans of Gulf War I [9] and the Vietnam War [10]. Increased rates of cardiac defects [11], decreased sperm counts and motility, and abnormal sperm morphology were also among the consequences of smoking cigarettes [12]. Whereas coculture of human sperm with benzo(a)pyrene (BP) produced premature acrosome reactions and accelerated hyperactivation, BP-exposed human males were found to have dysmorphic sperm and reduced sperm counts [13]. Similarly, wild-type mice exposed to daily BP exhibited low sperm counts and subfertility that extended to subsequent generations [14]. Moreover, mice lacking indoleamine 2,3-dioxygenase have significant increases in proinflammatory markers and in the number and percentage of morphologically abnormal sperm. Indoleamine 2,3-dioxygenase is the rate-limiting enzyme in the conversion of dietary tryptophan to kynurenic acid, which has an affinity for AHR that is comparable to that of 2,3,7,8-tetrachlorodibenzo-p-dioxin (TCDD) [15–17]. Although no direct mechanisms have been identified, collectively these findings suggest that either the absence of AHR ligand binding or AHR activation may result in inflammation, apoptosis, and oxidative stress in sperm leading to DNA damage [18, 19].

Despite the reproductive effects noted above, the role of AHR in spermatogenesis has received little attention. Normal cellular processes, such as the cell cycle, stem cell proliferation, and tissue differentiation, are regulated by AHR, and AHR is expressed in tissue-specific and developmental stage-specific patterns [20]. AHR expression in the seminiferous tubule was explored in the rat, where it was found to be restricted to the primary pachytene spermatocytes during stages VII–XI and round spermatids during stages II–XIV of the spermatogenic cycle. In contrast AHR and ARNT were expressed in all seminiferous tubule stages of the human testes [21]. Although male fertility, sperm count, seminal vesicle weight, and dorsolateral prostate weights are all decreased in *Ahr*-deficient mice in an age-dependent manner [22–24], no studies have documented the histological and gene expression consequences of *Ahr* loss of function on spermatogenesis. Here we have used the *Ahr* knockout (*Ahr*$^{-/-}$) mouse to gain insight into the role of AHR during spermatogenesis and fertilization.

[1]This material is based upon work supported by the Department of Veterans Affairs, Veterans Health Administration, Office of Research and Development, Health Services Research and Development. The views expressed in this article are those of the authors and do not necessarily reflect the position or policy of the Department of Veterans Affairs or the United States government.
[2]Correspondence: Kelle H. Moley, Department of Obstetrics and Gynecology, Washington University, School of Medicine, 660 South Euclid Ave, Campus Box 8064, St. Louis, MO 63110.
E-mail: moleyk@wustl.edu

Received: 24 February 2013.
First decision: 18 March 2013.
Accepted: 17 October 2013.

eISSN: 1529-7268 http://www.biolreprod.org
ISSN: 0006-3363

MATERIALS AND METHODS

Animals and Tissue Sampling

All the animal procedures were approved by both the Animal Studies Committee at Washington University in St. Louis and the Institutional Animal Care and Use Committee at the VA St. Louis Health Care System and were conducted in accordance with the specifications of the Taconic Farms (Hudson, NY) material transfer agreement. All the assays used 8–10 wk old *C57BL/6J Ahr^{b-1}* (WT) (Jackson Laboratories) and age-matched *C57BL/6-Ahrtm1.2Arte* homozygous *Ahr* deletion (*Ahr$^{-/-}$*) male mice (Taconic Farms). The Taconic *Ahr$^{-/-}$* mouse has a complete deletion of exon 3 that results in out of frame splicing and the absence of AHR functional protein. WT females that were 4-wk old were used as oocyte donors for in vitro fertilization (IVF). The animals were maintained on a 12L:12D cycle with free access to food and water.

Histology and Terminal Deoxynucleotidyl Transferase-Mediated dUTP Nick-End Labeling

Testes were fixed in Bouin solution, embedded in paraffin, and cut into 5-μm thick sections followed by hematoxylin and eosin (H&E) staining. For terminal deoxynucleotidyl transferase-mediated dUTP nick-end labeling (TUNEL), sections were deparaffinized in xylene for 15 min, rehydrated in ethanol grades, and hydrated in distilled water for 5 min. Sections were then treated with proteinase K (20 μg/ml) for 30 min at room temperature, rinsed with PBS and processed to detect fragmented DNA by using the In Situ Cell Death Detection Kit (Roche Diagnostics) according to the manufacturer's directions. Nuclei were counterstained with To-Pro 3 (1:500; Life Technologies) for 3 min. Label solution without terminal transferase was used for the negative control. The number of TUNEL-positive cells within the seminiferous tubule cross-sections was counted to determine the incidence of apoptosis in the WT and *Ahr$^{-/-}$* testes. Because fewer than nine apoptotic cells typically occur in the WT seminiferous tubule cross-sections [25], the prevalence of TUNEL-positive seminiferous tubules was represented as a percentage of the total number of seminiferous tubules with more than nine TUNEL-positive cells per seminiferous tubule cross-section. Approximately 500 to 600 tubules were counted per animal.

RNA Isolation and cDNA Synthesis

Testes were dissected and immediately immersed in optimal cutting temperature compound surrounded by dry ice and isopenthane and stored at −80°C. Total RNA was extracted with Trizol reagent (Life Technologies). RNA quantity and quality were confirmed via Nanodrop. RNA samples with 260 nm:280 nm ratios $\geq$1.8 were used for further analysis. RNA was reverse transcribed by using the QuantiTect reverse transcription kit (Qiagen) according to the manufacturer's recommendations.

Quantitative Real-Time PCR Analysis

Relative quantification of gene expression was determined via quantitative real-time PCR (qRT-PCR) by using the ABI 7500 fast and TaqMan gene expression assays (Applied Biosystems, Inc.) in accordance with the Minimum Information for Publication of Quantitative Real-Time PCR Experiments guidelines [26]. Expression of each candidate gene, no-template control, positive control, and the endogenous reference gene β-*actin* [27, 28] was analyzed by using equal amounts of input template. Complementary DNA prepared from adult mouse whole testis RNA (Agilent) was used for serial dilutions and standard curve analysis of each target gene and β-*actin* to ensure amplification efficiencies of 95% to 100%. The cDNA, 100 nM of gene-specific primers, and the TaqMan probe mix were amplified as follows: 95°C for 20 sec, then 40 cycles of 3 sec at 95°C and 30 sec at 60°C. Changes in gene expression were analyzed via relative quantification, and ΔC_t was calculated by subtracting the mean C_t of the endogenous controls from the C_t of the WT (reference samples) and *Ahr $^{-/-}$* target genes. The value for $\Delta\Delta C_t$ was ascertained through the subtraction of the WT ΔC_t from the ΔC_t of the *Ahr$^{-/-}$* target genes with WT (reference samples) values being set to one. Fold changes were calculated via $2^{-\Delta\Delta Ct}$. With the exception of spermatogenic-specific genes such as Melanoma antigen family A4 (*Magea4*), *Testin*, heat shock protein 2 (*HspA2*), and the protamines, WT liver was used as the positive tissue control. The representative genes, corresponding TaqMan assay ID numbers, and amplicon sizes appear in Table 1.

Sequence Analysis

DNA sequence for ~10.4 kb upstream of mouse *Testin*, and ~5.5 kb upstream of mouse *Magea4*, including the genes, was extracted from the UCSC Genome Browser (http://genome.ucsc.edu/) [29] and searched for the AHR response element (AHRE) core consensus site 5′-T/NGCGTG-3′ [30] in DNASTAR Seqbuilder v11.0.

Western Blot Analysis

Proteins were extracted from caudal sperm, liver, testes, and epididymis and analyzed by Western blot analyses according to standard procedures. The primary antibodies were anti-AHR (1:1000; Enzo Life Sciences), anti-MAGEA4 (1:1000; Sigma), and anti-TESTIN (1:1000; Protein Tech). Horseradish peroxidase-conjugated goat-anti-rabbit, goat-anti-mouse, or donkey anti-goat secondary antibodies (1:15 000; Santa Cruz Biotechnology) and Super Signal West Femto Maximum Sensitivity Chemiluminescence Substrate (Thermo Scientific) were used for detection. The loading control was β-tubulin (1:1000; Santa Cruz Biotechnology).

AHR Immunofluorescence

Four different anti-AHR antibodies and several different fixation conditions were tested to identify a method that resulted in minimal nonspecific staining in testes from *Ahr*-null mice. Testes were fixed in modified Davidson fixative, embedded in paraffin, cut into 5-μm thick sections, deparaffinized, and rehydrated. After antigen unmasking with 10 mM sodium citrate, pH 6.0, sections were blocked at room temperature for 30 min in 5% nonfat dry milk powder in Tris-buffered saline (50 mM Tris-Cl, pH 7.5, 150 mM NaCl [Sigma]). The sections were incubated overnight at 4°C with rabbit polyclonal anti-AHR (1:50; Enzo Life Sciences), incubated for 1 h with the Alexa Fluor 488 goat-anti-rabbit (1:400; Life Technologies), and incubated for 5 min with Sytox Orange (1:1000; Life Technologies) as the counterstain.

Sperm from the cauda epididymis were allowed to swim freely for 15 min in VitroFert Cook Medical), transferred to microtubes, and pelleted for 5 min at 500 relative centrifugal force. After resuspending the pellets in 5 ml of VitroFert, the sperm were allowed to swim up for 45–60 min at 37°C under 5% CO_2 incubation. The supernatant was then collected, pelleted, and applied to slides. The slides were fixed for 3 min at room temperature in 4% paraformaldehyde, blocked for 1 h in bovine serum albumin and normal goat serum, permeabilized in Triton X-100 and PBS for 30 min, and washed with PBS. Primary and secondary antibody incubation was completed as described above, and TO-PRO 3 (1:500; Life Technologies) was used as the nuclear counterstain. Negative controls, without primary antibodies, were used to confirm nonspecific reactions.

Oocyte Retrieval, Sperm Preparation, and IVF

A 1:5 male to female ratio of 8- to 10-wk-old WT or age-matched *Ahr$^{-/-}$* males and 4-wk-old WT superovulated (Jackson Laboratories) females was used for IVF. Superovulation occurred via a one-time intraperitoneal injection of 5 international units of pregnant mare serum gonadotropin, followed by 5 international units of human chorionic gonadotropin (HCG) 48 h later. At 12–13 h post-HCG injection, sperm were prepared from appropriate males as follows: the testes and epididymis were quickly dissected, the testes snap frozen, and the sperm recovered from the cauda epididymis. A few incisions were made in the cauda epididymis, and the sperm were gently teased out. A fraction of the sperm was removed for immunofluorescence, morphology analysis (Spermac stain; FertiPro, N.V.), or computer-assisted semen analysis (Hamilton-Thorne Research) to determine motility and average concentration. Sperm were capacitated by incubating in 500 μl of VitroFert (Cook Medical) for 90 min at 37°C under 5% CO_2. At 14–15 h post-HCG injection, the oviducts were dissected, the cumulus oocyte complexes were removed from the ampulla, and a standardized aliquot ($<$10 μl of 2×10^6 sperm/ml) of sperm was added to the insemination dish. After 4–6 h, the fertilized oocytes were triple washed in EmbryoMax Potassium Simplex Optimized Medium with 1/2 Amino Acids (Millipore Corporation) and incubated at 37°C in a 5% CO_2, 5% O_2, 90% N_2 modular incubator (Billups-Rothenberg). Two-cell (fertilization rate) and Embryo Day 3.5 blastocyst rates were determined by counting. No embryos were transferred into recipient females.

Sperm Morphology

Sperm were collected as described above and allowed to swim freely in VitroFert for 5 min at 37°C under 5% CO_2 incubation. Spermac (SPS050; FertiPro, N.V.) fixative and stain were used according to the manufacturer's

TABLE 1. TaqMan assays used for qRT-PCR analysis.

No.	Name	Ref. sequence	TaqMan assay ID	Amplicon size (base pairs)
1	Aryl hydrocarbon receptor (*Ahr*)	NM_013464.4	Mm01291777_m1	98
2	Aryl hydrocarbon receptor repressor (*Ahrr*)	NM_009644.2	Mm01352370_m1	98
3	β-actin (*Actb*)	NM_007393.3	Mm00607939_s1	115
4	Cytochrome P4501A1 (*Cyp1A1*)	NM_001136059.1	Mm00487218_m1	120
5	Heat shock-related 70-kDa protein 2 (*Hspa2*)	NM_008301	Mm00434069_s1	62
6	Heat shock protein HSP 90-alpha (*Hsp90aa1*)	NM_010480	Mm00658568_gH	128
7	Melanoma antigen, family A, 4 (*Magea4*)	NM_020280	Mm00522322_s1	103
8	Nuclear factor, erythroid derived 2, like 2 (*Nrf2*)	NM_010902.3	Mm00477784_m1	61
9	cyclin-dependent kinase inhibitor 1A (*P21*)	NM_007631.2	Mm00432359_m1	58
10	Protamine 1 (*Prm1*)	NM_013637	Mm00726976_s1	102
11	Protamine 2 (Prm2)	NM_008933	Mm00656902_g1	153
12	Superoxide dismutase 1 (*Sod1*)	NM_011434	Mm01700393_g1	85
13	Superoxide dismutase 2 (*Sod2*)	NM_013671	Mm00449725_g1	108
14	Testis-derived transcript (*Testin, Tes*)	NM_207176.3	Mm03053485_s1	123
15	Uncoupling protein 2 (mitochondrial, proton carrier) (*Ucp2*)	NM_011671	Mm00627598_m1	89

directions. The slides were viewed under 400× and 1000× oil immersion by one primary unblinded reviewer and two independent blinded reviewers. One hundred sperm were counted per slide per animal for a total of 300 WT sperm and 300 *Ahr* $^{-/-}$ sperm. Morphology was classified as normal or abnormal on the basis of the characteristics of the head and tail, or the presence of a cytoplasmic droplet [31]. Abnormalities were counted as aggregate percentages.

Statistical Analyses

For qRT-PCR data, mean threshold cycle (C_t) values were analyzed relative to the mean (C_T) of the endogenous control β-*actin* to generate ΔC_t, which was subsequently normalized to one (WT) as the reference sample to generate $\Delta\Delta C_t$. The results were then log transformed ($2^{-\Delta\Delta Ct}$) and presented as ± fold change. Quantitative real-time PCR data are presented as the mean ± SEM of four independent experiments, each assayed in duplicate. Statistical significance of the qRT-PCR data was determined via one-way ANOVA (nonparametric) with 95% confidence intervals. The fertilization percentage was determined by dividing the number of two-cell embryos by the number of ova. The percent of two-cell embryos that developed into blastocyst-stage embryos was calculated by dividing the number of blastocysts by the number of initial two-cell embryos. Reproductive data and organ weights are expressed as the mean of three independent experiments. Differences were analyzed by using unpaired *t*-tests; $P < 0.05$ was considered statistically significant. Sperm morphology and immunofluorescence were verified by independent observation.

RESULTS

The AHR Is Required for Normal Spermatogenesis

Because of the comparatively stable testis weight within a species [32], a significant increase or decrease in reproductive organ weights may reflect damage to the seminiferous epithelium and be indicative of an adverse reproductive effect. When compared to WT control, the reduced body weight and relative testis to body weight in the *Ahr*$^{-/-}$ males were nonsignificant. In comparison, the reduced weights of the *Ahr*$^{-/-}$ testis, epididymis, and cauda epididymis weights were highly significant with *P*-values of 0.004, 0.003, and 0.009, respectively. The relative epididymis to testis weight (30.4% ± 0.6% vs. 37.2% ± 1.9 %) was also significantly lower ($P < 0.05$) in *Ahr*$^{-/-}$ when compared to WT controls (Table 2). Given the alterations in the reproductive organ weights, we completed a thorough histopathological evaluation of the seminiferous epithelium and observed a number of abnormalities in those from *Ahr*$^{-/-}$ males (Fig. 1). H&E staining of the stages VII–VIII *Ahr*$^{-/-}$ cross-sections revealed hypocellularity with widened intercellular spaces, multinucleated giant cells, and vacuoles suggesting missing germ cell stages (Fig. 1A). The cleavage of spermatocytes from round spermatids was also noted in the stages VII–VIII *Ahr*$^{-/-}$ cross-sections (Fig. 1C), which was consistent with sloughing of the apical region of the seminiferous epithelium. At stage XII, there were excess numbers of retained spermatids in the basal compartment of the seminiferous epithelium of the *Ahr*$^{-/-}$ mice (Fig. 1E), which suggested the failure of spermatids to disengage during spermiation [33]. Widened intercellular spaces were again noted at stages IV–VI of the H&E stained *Ahr*$^{-/-}$ cross sections (Fig. 1E). Collectively, these findings were indicative of seminiferous epithelial degeneration, disrupted germ cell attachment, insufficient structural support, and the failure of the spermatids to detach from the Sertoli cells during spermiation.

To examine whether there was excess cell death in the *Ahr*$^{-/-}$ testes, we used TUNEL to examine the numbers of apoptotic cells. Compared to WT, there was a significant increase ($P < 0.05$) in the percentage of TUNEL-positive seminiferous tubules (64% vs. 3%) in the *Ahr*$^{-/-}$ cross-sections (Fig. 2, A and B).

Gene Expression Changes in Testes Lacking AHR

To confirm that the *Ahr*$^{-/-}$ mice did not express *Ahr* in the testis and to examine the expression of other genes in the classic AHR pathway, we performed qRT-PCR on RNA isolated from *Ahr*$^{-/-}$ and WT testes, epididymis, and caudal sperm. The WT liver was the positive tissue control. As

TABLE 2. Absolute and relative body and reproductive organ weights.

Parameter	WT (n = 3)*	*Ahr*$^{-/-}$ (n = 3)*	*P* value
Body weight	25.033 ± 0.433 g	23.6 ± 0.5 g	0.096
Testis weight	92.8 ± 0.85 mg	78.4 ± 0.2.2 mg	0.004
Testis/body weight	0.371% ± 0.010%	0.332% ± 0.017%	0.118
Epididymis weight	34.6 ± 1.68 mg	27.3 ± 0.248 mg	0.003
Epididymis/testis weight	37.2% ± 1.91%	30.4% ± 0.61%	0.027
Cauda epididymis weight	10 ± 0.7 mg	6.3 ± 0.3 mg	0.009

* All the values are mean ± SEM.

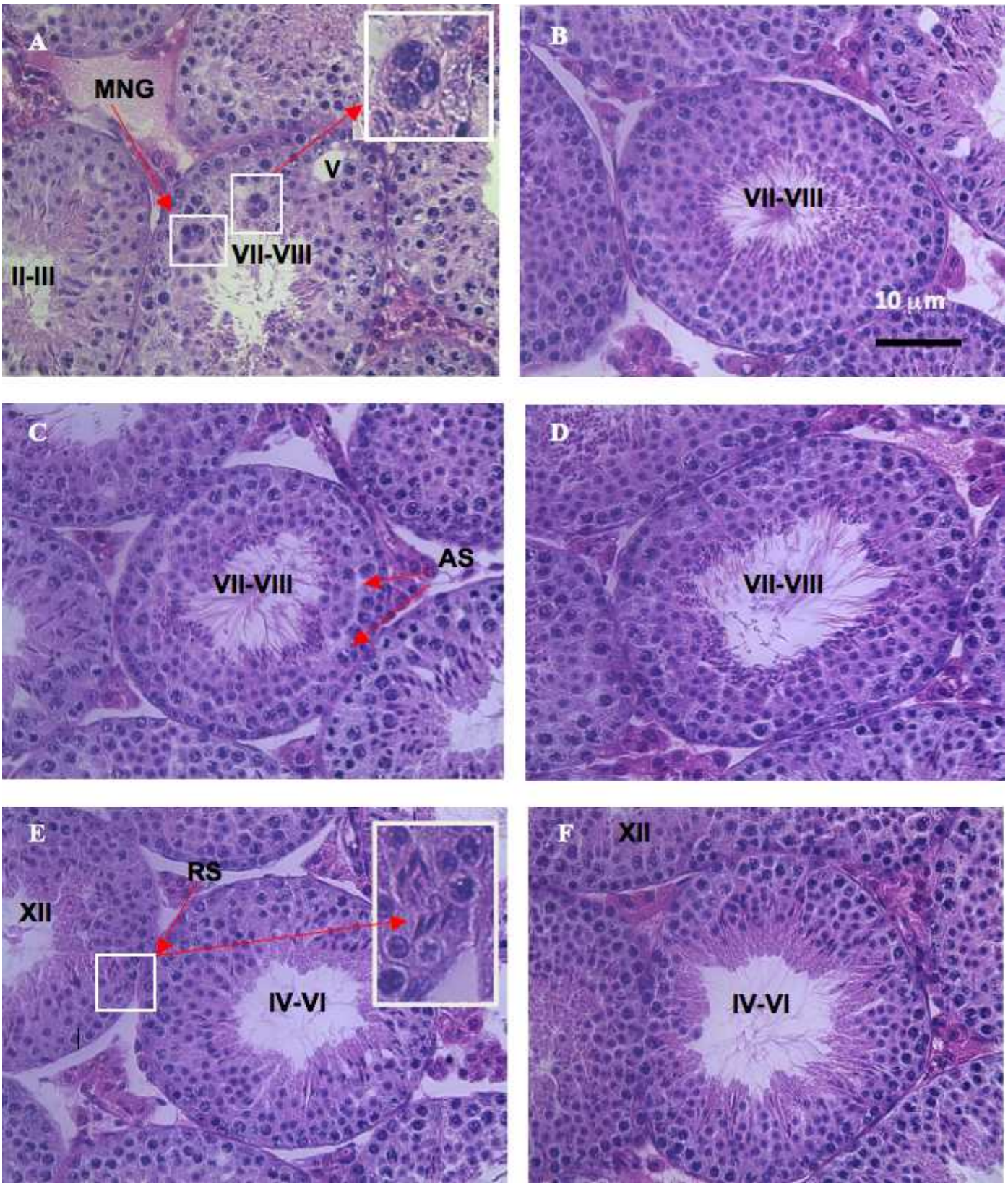

FIG. 1. The seminiferous epithelium is disrupted in *Ahr*$^{-/-}$ mice. H&E staining in sections of the seminiferous epithelium from *Ahr*$^{-/-}$ (**A**, **C**, and **E**) and WT (**B**, **D**, and **F**) mice. Boxed regions are shown at higher magnifications in insets. Stages of spermatogenesis (II–III, IV–VI, and VII–VIII) are indicated. Multinucleated giant cells (MNG) and vacuoles (V) are highlighted in **A**. Apical sloughing (AS) is pointed to in **C**. Retained spermatids (RS) in **E**. Bar = 10 μm.

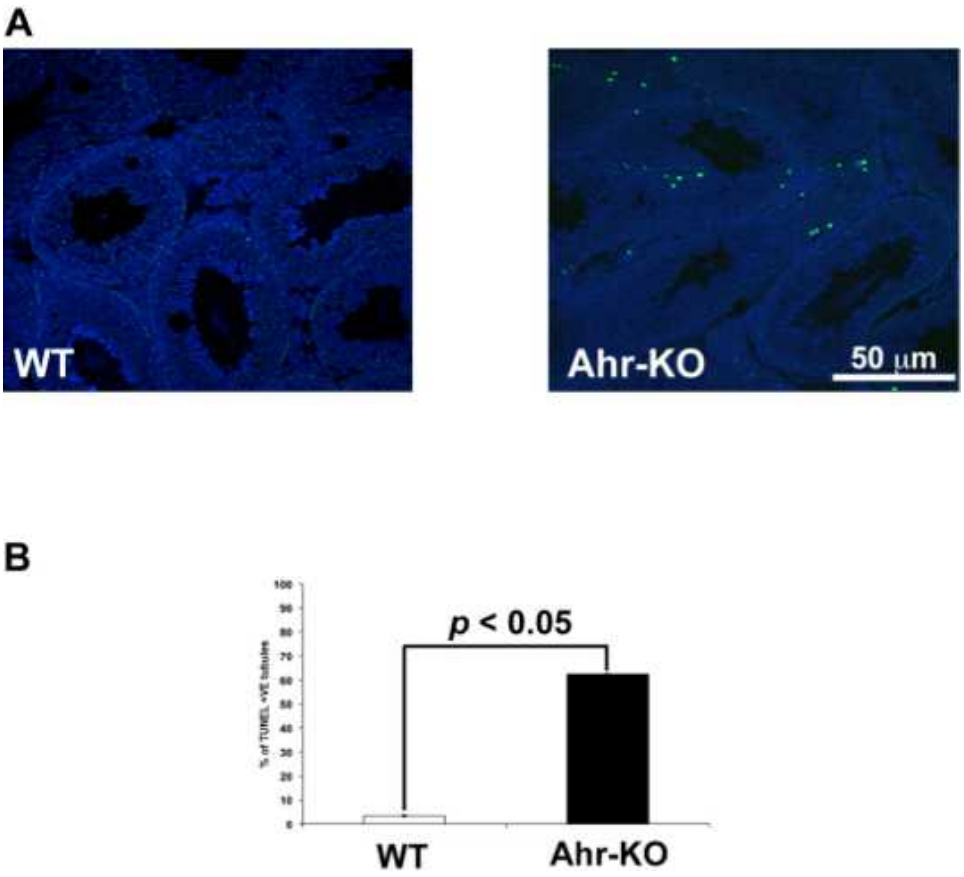

FIG. 2. Apoptosis in the seminiferous epithelium is increased in $Ahr^{-/-}$ (Ahr-KO) mice. **A**) Testes from WT and $Ahr^{-/-}$ mice were assessed for cell death by TUNEL (green labeling indicative of TUNEL-positive cells). **B**) Histogram represents the quantitation of TUNEL-positive apoptotic cells (green) and nuclear staining (blue) in $Ahr^{-/-}$ and WT seminiferous tubules. The incidence of apoptosis in WT and $Ahr^{-/-}$ testis sections was determined by counting the number of TUNEL-positive cells (green) within a seminiferous tubule cross-section. The data were presented as the percentage of seminiferous tubules containing more than nine apoptotic cells of the total number of seminiferous tubules counted. Approximately 500–600 tubules were counted per animal. Results are presented as the mean ± SEM of three individual experiments; *P*-value indicates the significant difference in percent of apoptosis between WT and $Ahr^{-/-}$. See *Materials and Methods* for details of the quantitation method.

expected, *Ahr* was significantly down-regulated in all $Ahr^{-/-}$ tissues examined. There was a 32-fold reduction in *Ahr* when compared to WT testes (Fig. 3A). We also examined the expression of two transcriptional targets of AHR, AHR repressor *(Ahrr)* and *Cyp1A1*, and found that expression of these genes was undetectable in WT caudal sperm or the epididymis. *Ahrr* and *Cyp1A1* were expressed at a significantly lower level in testes from $Ahr^{-/-}$ mice than in testes from WT mice (Fig. 3, B and C). By contrast, expression of *Hsp90*αα*1,* which is a subclass of *Hsp90*α and encodes a chaperone protein for a variety of proteins, including AHR [34], but is not a known transcriptional target of AHR, was unaffected by loss of *Ahr* in the liver and whole testes but was lower in sperm (Fig. 3D). *Hsp90*α homozygous mutant mice were also reported to be sterile with defects in spermatogenesis [35]. While there are two subclasses of *Hsp90a*, the functions are rarely differentiated. Because the expression of *Hsp90aa1* surpassed that of *Hsp90aa2* in all spermatogenic cell stages [35, 36], *Hsp90aa1* was selected as the isoform for this study.

To begin to understand why loss of AHR led to the defects we observed in seminiferous tubules, we examined expression levels of candidate genes involved in cell cycle regulation and cell-cell adhesion. Because the seminiferous epithelium accounts for 80% of the weight of the adult testis [37], whole testis mRNA was used as a surrogate marker of gene expression in seminiferous epithelium. *Magea4* is a growth-promoting gene that inhibits cell cycle arrest and p53-mediated apoptosis [38] and that is completely silent in normal tissues with the exception of type A and B spermatogonia, some tumor cells, and the placenta [39–41]. *Magea4* expression was 4-fold lower in $Ahr^{-/-}$ testes ($P < 0.05$) than in WT testes. We next examined the expression of *P21,* which is a negative regulator of the cell cycle, is weakly expressed in spermatocytes and spermatids, and is induced by AHR activation [42]. However, expression of *P21* was not significantly affected by the loss of AHR in the testis (not shown), suggesting that cell cycle regulation was intact. Finally, consistent with the idea that the histological defects we observed were due to Sertoli cell degeneration, *Testin,* a specific marker of Sertoli cell and germ cell adhesion [43], was more than 100-fold lower in $Ahr^{-/-}$ testes ($P < 0.01$) than in WT testes (Fig. 4),

Because depleted germ cells typically cause a physiologic surge of TESTIN [44] and the dramatic down-regulation of *Testin* was inconsistent with the histopathology, we therefore wondered whether *Testin* was regulated by AHR. Using the UCSC genome browser [29], we found 35 core AHRE within 9 kb of the *Testin* start site and two AHRE (−73 and −54) located within the region (−425 to + 58) of maximal *Testin* promoter activity [44]. The presence of multiple copies of AHRE suggested the possibility that *Testin* is highly regulated by AHR. Conversely *Magea4* contains only one AHRE at position +590 in this single exon gene.

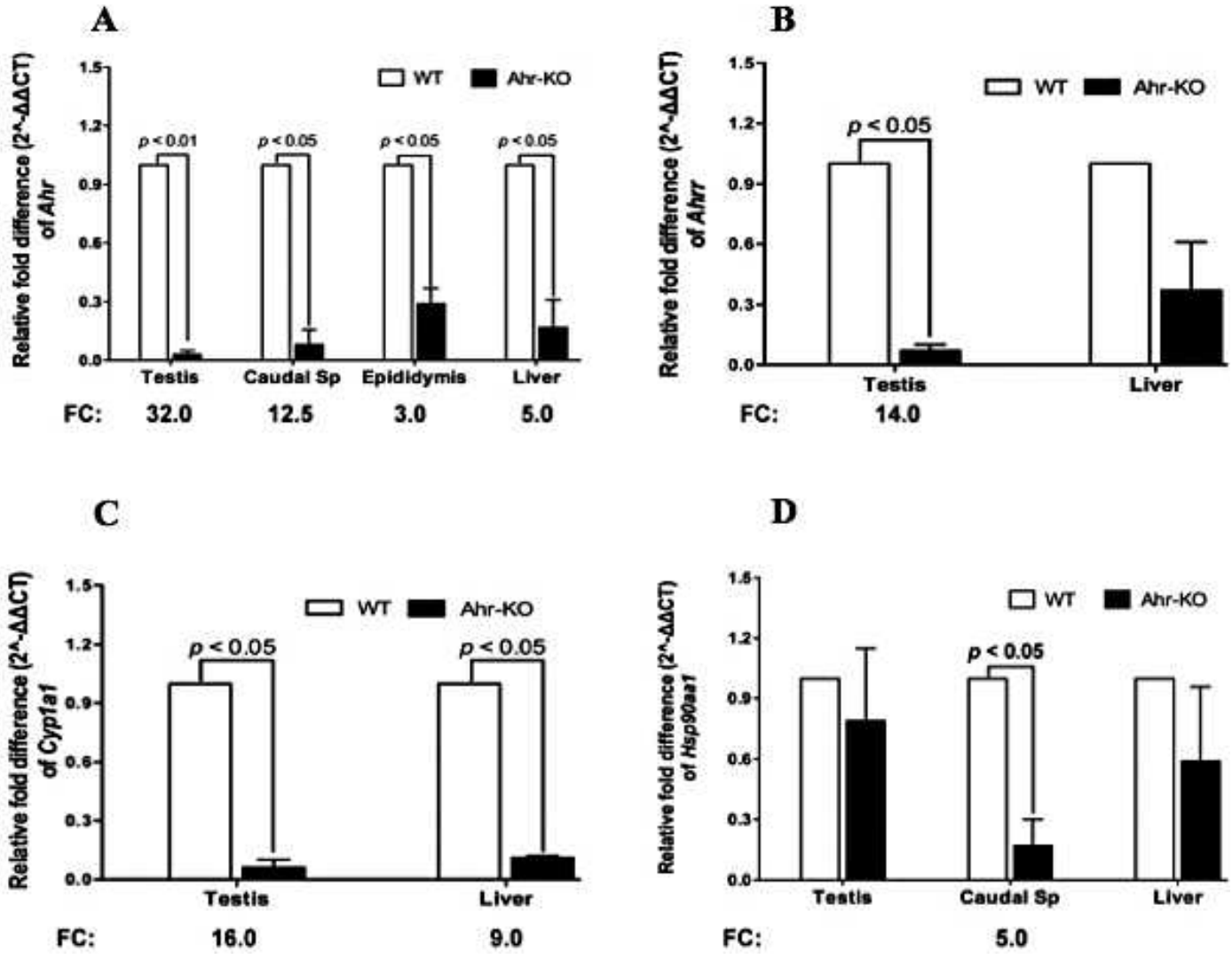

FIG. 3. Analysis of the AHR pathway in the testis by qRT-PCR. Histograms represent the relative fold difference in expression of the indicated genes between WT and $Ahr^{-/-}$ (Ahr-KO) testes, caudal sperm, and liver (positive control). The qRT-PCR data were normalized against the reference genes, β-actin and β_2-microglobulin, and converted to relative fold difference of mRNA expression of the candidate genes. Fold changes (FC) were calculated via $2^{-\Delta\Delta Ct}$ and represent the down-regulation of the $Ahr^{-/-}$ candidate genes compared to the WT reference sample, which has a final value of one. Only the fold changes indicative of significant down-regulation ($P < 0.05$) appear below the corresponding genes. **A**) The 32-fold down regulation of *Ahr* in the $Ahr^{-/-}$ testis. **B** and **C**) The 14-fold and 16-fold down regulation of *Ahrr* and *Cyp1A1*, respectively, in the testis of the $Ahr^{-/-}$ mouse. Data are expressed as the mean ± SEM of four independent experiments, each assayed in duplicate.

Given the histological abnormalities in the $Ahr^{-/-}$ seminiferous tubules, we examined the expression of genes that are expressed during spermiogenesis. *Prm1* and *Prm2* encode protamines, which replace histones late in spermatogenesis and are responsible for sperm head condensation. *Hspa2* encodes a heat shock protein that is expressed exclusively in spermatogenic cells (reviewed in [45]) and is a chaperone of transition proteins that precede protamination. Disrupted HSPA2 is associated with poorly remodeled germ cells with residual mitochondria that generate increased reactive oxygen species [46]. All three of these genes were expressed at lower levels in $Ahr^{-/-}$ testes than in WT testes (Fig. 5).

Because activation of AHR causes oxidative stress, we examined the expression of several genes involved in response to this insult. Uncoupling protein 2 (UCP2) controls the formation of mitochondrial reactive oxygen species [47], superoxide dismutase (SOD, encoded by *Sod1* and *Sod2*), rapidly converts the superoxide free radical to hydrogen peroxide for rapid elimination [18], and the transcription factor NRF2 coordinates the rapid cellular response to oxidative stress [48]. *Ucp2*, *Sod2*, and *Nrf2* were all expressed at lower levels in $Ahr^{-/-}$ testes than in WT testes (Fig. 6). Taken together, our gene expression studies suggest the presence of poorly remodeled germ cells with increased vulnerability to oxidative stress in $Ahr^{-/-}$ mice.

The AHR Is Required for Proper Sperm Morphology and Function

Because oxidative stress is thought to play a significant role in DNA damage in sperm and thus may affect fertilization [18], we next asked whether the histological and gene expression abnormalities we observed in the testis corresponded with defects in mature sperm. We first isolated caudal sperm from WT and $Ahr^{-/-}$ mice and used qRT-PCR to confirm that *Ahr* and *Hsp90αα1* are expressed in WT sperm and demonstrate that expression of these genes is significantly decreased in $Ahr^{-/-}$ sperm (Fig. 3). Subsequent immunofluorescence

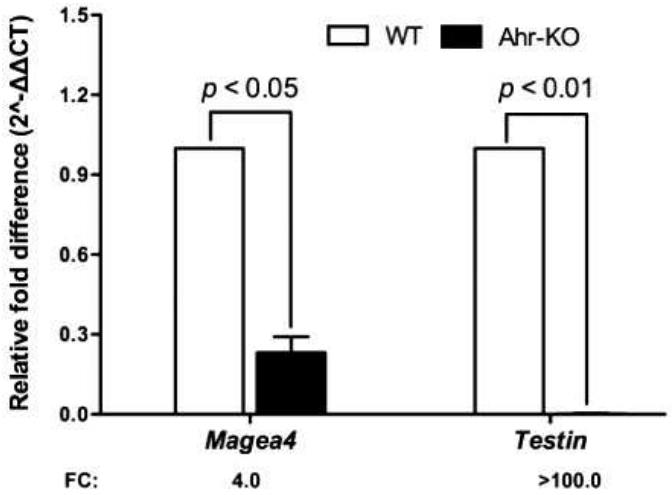

FIG. 4. Expression of genes involved in cell proliferation and cell-cell adhesion is affected by loss of *Ahr*. Histograms represent the relative fold difference in expression of the *Magea4* and *Testin* between WT and $Ahr^{-/-}$ (Ahr-KO) testes as described in Figure 3. Data are expressed as the mean ± SEM of four independent experiments, and each is assayed in duplicate.

analysis revealed that AHR localized to the acrosome and the principal piece of the sperm flagella in WT sperm when compared to the $Ahr^{-/-}$ sperm (Fig. 7). AHR disappeared from the WT sperm acrosome postcapacitation (data not shown). While the mean background rate of abnormal sperm in this study was 30.5%, the prevalence of abnormalities in the $Ahr^{-/-}$ sperm approached 42.6% (Fig. 8), Abnormalities included flattening of the base of the head, loss of the typical hook-shaped head, changes in the flagellum such as a folded or coiled tail, and the presence of a cytoplasmic droplet [31]. Sperm concentration and sperm motion parameters were then quantified by computer-assisted sperm analysis. Sperm count, average motility, and progressive motility were not significantly different between $Ahr^{-/-}$ and WT mice (Table 3).

To determine whether $Ahr^{-/-}$ sperm were functional, we performed IVF with oocytes from WT females. IVF is ideal because of the ability to eliminate the influence of seminal fluid factors and analyze pure sperm populations devoid of somatic cell contamination; any differences that are seen are thus unambiguously sperm-specific. The mean IVF rate (as measured by formation of two-cell embryos) was significantly lower ($P < 0.05$) with sperm from $Ahr^{-/-}$ males than with sperm from WT controls (48.6% vs. 80.6%). In contrast, the progression of two-cell embryos to blastocyst-stage embryos from the $Ahr^{-/-}$ males was significantly higher ($P < 0.05$) when compared to WT controls (Fig. 9).

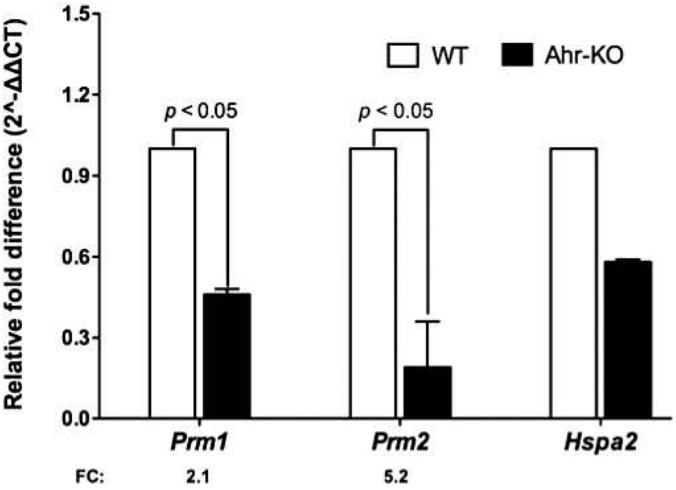

FIG. 5. Expression of genes involved in sperm chromatin condensation is affected by loss of *Ahr*. Histograms represent the relative fold difference in expression of the *Prm1, Prm2,* and *Hsp70a* between WT and $Ahr^{-/-}$ (Ahr-KO) testes as described in Figure 3. Data are expressed as the mean ± SEM of four independent experiments, and each is assayed in duplicate.

Protein Expression in WT and $Ahr^{-/-}$ *Testes*

Modified Davidson was the preferred fixative, and rabbit polyclonal anti-AHR generated reproducible results. We were able to demonstrate that, in testes from WT mice, AHR was located in the Sertoli cell nucleus lying near the basement membrane, in the interstitium, and in the cytoplasm of the round spermatids. Additionally, we observed intense staining in the lumen of the seminiferous tubules as well as linear filamentous staining, suggesting the presence of AHR in the tail of the elongated spermatids (Fig. 10). To assess this possibility, we stained caudal spermatozoa and found that AHR localized to the acrosome and the principal piece of the sperm flagella in WT sperm (Fig. 7). AHR disappeared from the WT sperm acrosome postcapacitation (data not shown).

Because we observed some background AHR staining in the seminiferous tubules from $Ahr^{-/-}$ mice, we performed Western blot analyses to confirm that the protein was absent in the mutants. Consistent with the staining of caudal sperm (Fig. 7), we observed a faint band of the expected size (97 kDa) in extracts from WT caudal sperm. Additionally, we demonstrated that AHR is expressed in the testis, epididymis, and liver of WT males (Fig. 11). The lack of detectable bands in the corresponding samples from $Ahr^{-/-}$ mice indicates that the staining we observed in seminiferous tubules from $Ahr^{-/-}$ mice was nonspecific. Western blot analysis also confirmed that TESTIN and MAGEA4 protein was also reduced in testis from $Ahr^{-/-}$ mice (Fig. 11).

DISCUSSION

This study is the first to show that AHR is important to the structure and function of the seminiferous tubules. Our histological observations demonstrated that testes from $Ahr^{-/-}$ mice have significant architectural distortions at stages IV–XII of the seminiferous epithelium. The phenotypes we observed are suggestive of significant seminiferous epithelial degeneration and compromised Sertoli cell function. Sertoli cells extend from the basal lamina to the lumen of the seminiferous tubules to maintain direct and interactive contact throughout spermatogenesis until the detachment of the spermatozoa at spermiation [49]. Similar abnormal phenotypes (such as those described in this model) have been observed in the testes of mice exposed to mono-2-ethylhexyl phthalate, a male reproductive toxicant that selectively targets Sertoli cells and creates vacuolization and seminiferous epithelial disorganization, resulting in spermatocyte and spermatid degeneration [50]. In this study, AHR was observed in a Sertoli cell nucleus. This conforms to earlier reports of AHR immunoreactivity in Sertoli cells in the rat and human testes [21] and provides a mechanism whereby AHR ligands disrupt Sertoli cell functions. A single injection of TCDD led to widened spaces between germ cells and Sertoli cells in mice [23]. Additionally, the in vitro treatment of Sertoli cells with TCDD for 24 h led to the down-regulation of *Testin* and induction of *Cyp1A1*, which provided evidence of the activation of the AHR-signaling pathway [22, 51]. While it is seemingly inconsistent that both

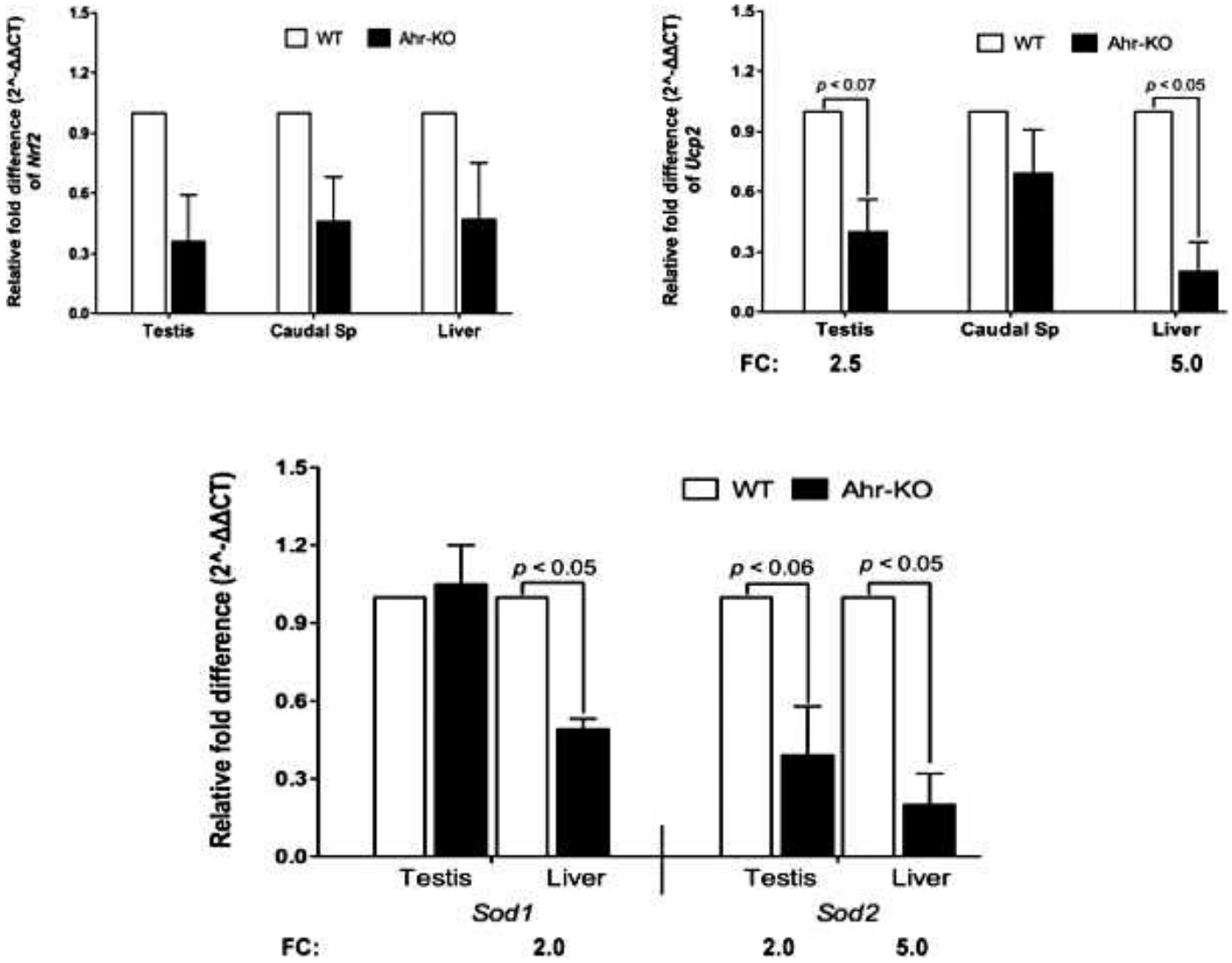

FIG. 6. Expression of genes involved in oxidative stress is affected by loss of *Ahr*. Histograms represent the relative fold difference in expression of the indicated genes between WT and $Ahr^{-/-}$ (Ahr-KO) testes, caudal sperm, and liver as described in Figure 3. Data are expressed as the mean ± SEM of four independent experiments, and each is assayed in duplicate.

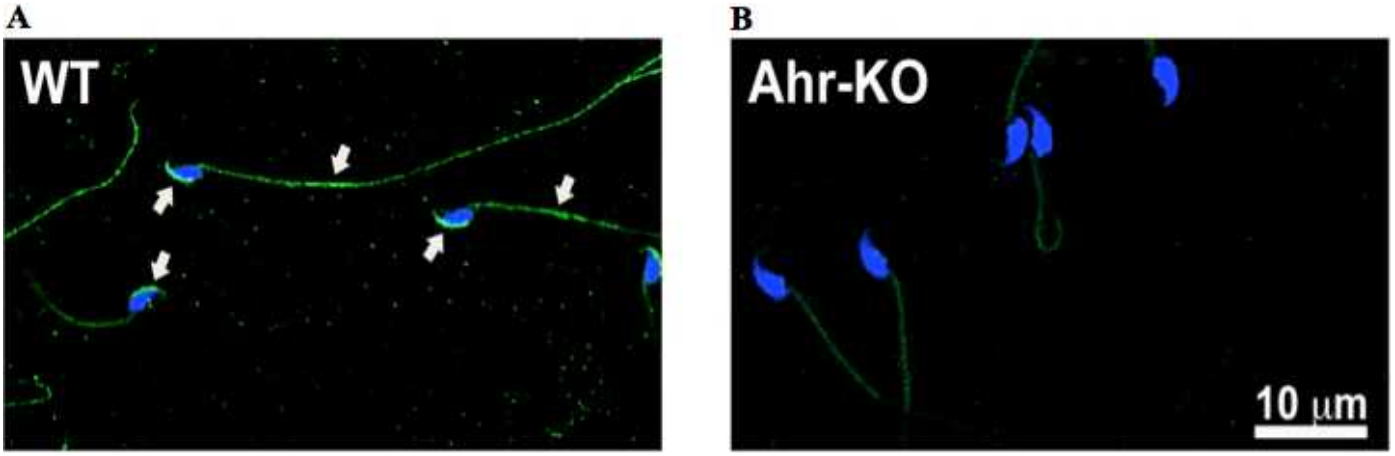

FIG. 7. The AHR in caudal spermatozoa. AHR protein (green) and nuclear (blue) staining of WT (**A**) and $Ahr^{-/-}$ (**B**) caudal sperm. **A**) AHR localization in the acrosome (arrows), and the principal piece of the flagellum, which was absent in the $Ahr^{-/-}$ sperm (**B**). Bar = 10 μm.

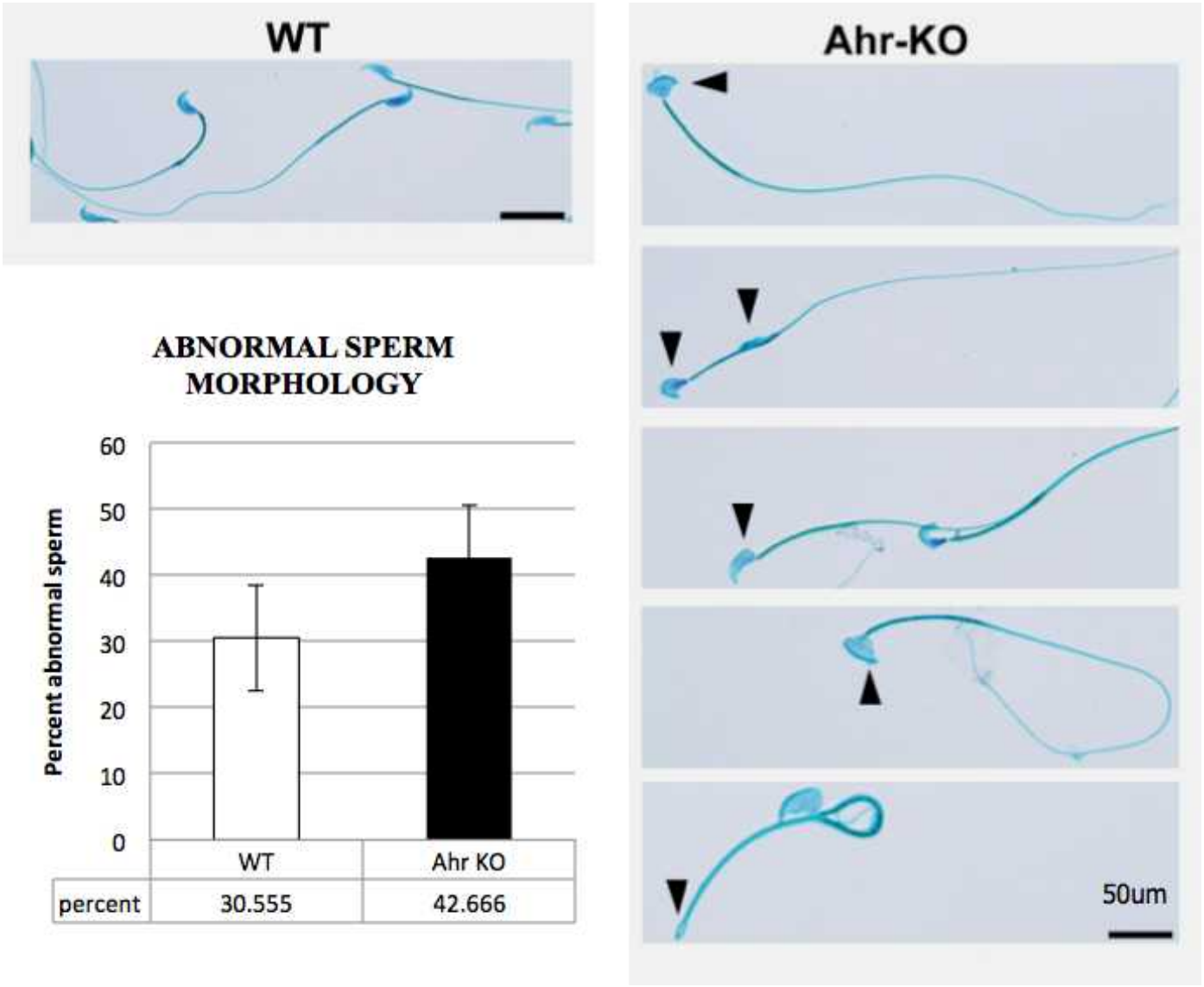

FIG. 8. Sperm morphology assessment in the $Ahr^{-/-}$ (Ahr-KO) mouse. Spermac fixative and staining were used for sperm morphology assessment. Abnormalities included flattening of the base of the head, loss of the typical hook-shaped head, changes in the flagellum such as a folded or coiled tail, and the presence of a cytoplasmic droplet. Percent of abnormal sperm are presented in the histogram. The background rate of WT sperm abnormalities was 30.5% (white bars) compared to 42.6% of $Ahr^{-/-}$ sperm. Bar = 50 μm.

AHR loss of function, as described in this study, or AHR activation can down-regulate *Testin*, the latter can potentially be explained by the rapid AHR protein degradation (half life of 3 h) that occurs in the presence of intense and continuous AHR ligand activation [52]. When considered within this context, the dramatic down-regulation of *Testin* coupled with multiple AHREs in the *Testin* promoter region and the histopathology of the $Ahr^{-/-}$ seminiferous tubule cross-sections support the conclusion that AHR modulates Sertoli-germ cell interactions. In addition to Sertoli cell defects, the results of our gene expression studies suggest that there are germ cell defects in $Ahr^{-/-}$ mice. The down-regulation of *Magea4* suggested

TABLE 3. Computer-assisted semen analysis parameters and fertility measures.

Parameter	WT (n = 3)[a]	$Ahr^{-/-}$ (n = 3)[a]	*P* value
Total concentration (10^6/ml)	1.24 ± 0.15	0.60 ± 0.175	0.052
Average motility (%)	49.83 ± 7.39	56.66 ± 5.95	0.511
Progressive motility (%)	22.58 ± 3.92	29.37 ± 2.12	0.291
Rapid velocity (%)	41.75 ± 5.43	50.16 ± 5.49	0.337
Fertility (%)[b]	80.67 ± 6.01	48.67 ± 5.36	0.016
Blastocysts (%)[c]	82.33 ± 2.33	90.67 ± 0.33	0.024

[a] Values are means ± SEM.
[b] Fertility defined as percentage of ova that developed into two-cell embryos.
[c] Blastocyst formation defined as percentage of two-cell embryos that developed into blastocysts.

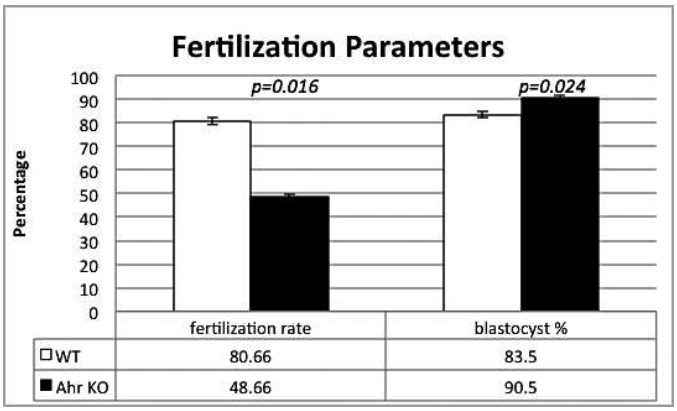

FIG. 9. Functional sperm analysis. The functional capacity of $Ahr^{-/-}$ (Ahr KO) sperm was measured by the two-cell embryo and blastocyst percentage compared to WT controls. The percentage of two-cell embryos (fertilization rate) is plotted; $*P < 0.05$ indicate the difference in expression between $Ahr^{-/-}$ and WT.

reduced spermatogonial proliferation, and the reduced expression of *HspA2*, *Prm1*, and *Prm2* indicate a defect in mature germ cell formation. Furthermore the single copy of AHRE within *Magea4* suggests that AHR may act as a coregulator but not as a transcriptional regulator.

AHR expression patterns in the testes are also species-specific and developmentally driven, with some seminiferous tubule stages completely devoid of AHR staining [7, 21]. While this was not unexpected, it complicated our attempts to distinguish AHR WT by immunofluorescence using the $Ahr^{-/-}$ mouse as the negative control. Four different antibodies were therefore tried using WT and $Ahr^{-/-}$ livers as the positive and negative controls, respectively. The rabbit polyclonal anti-AHR from Enzo Life Sciences was found to be reliable by Western blot analysis and provided reliable immunofluorescence with results that paralleled published data [21]. However, the filamentous staining and the intense AHR signal in the WT lumen were previously unreported and supported the presence of AHR on the WT sperm flagella.

Our results also indicate that AHR plays a role in the formation of fully functional mature sperm. We present the first evidence that AHR is localized in the acrosome and the principal piece of the sperm flagellum. Staining of the sperm tails was observed both in isolated sperm and in testis cross-sections. Our qRT-PCR data also supports our conclusion that *Ahr* is expressed in mature sperm. Given that numerous drugs and other compounds have been found in human seminal fluid [53], AHR may contribute to xenobiotic metabolism in sperm and may be important for fertilization. For example, the AHR ligand TCDD can increase intracellular calcium concentration [54], which could affect sperm capacitation. Consistent with

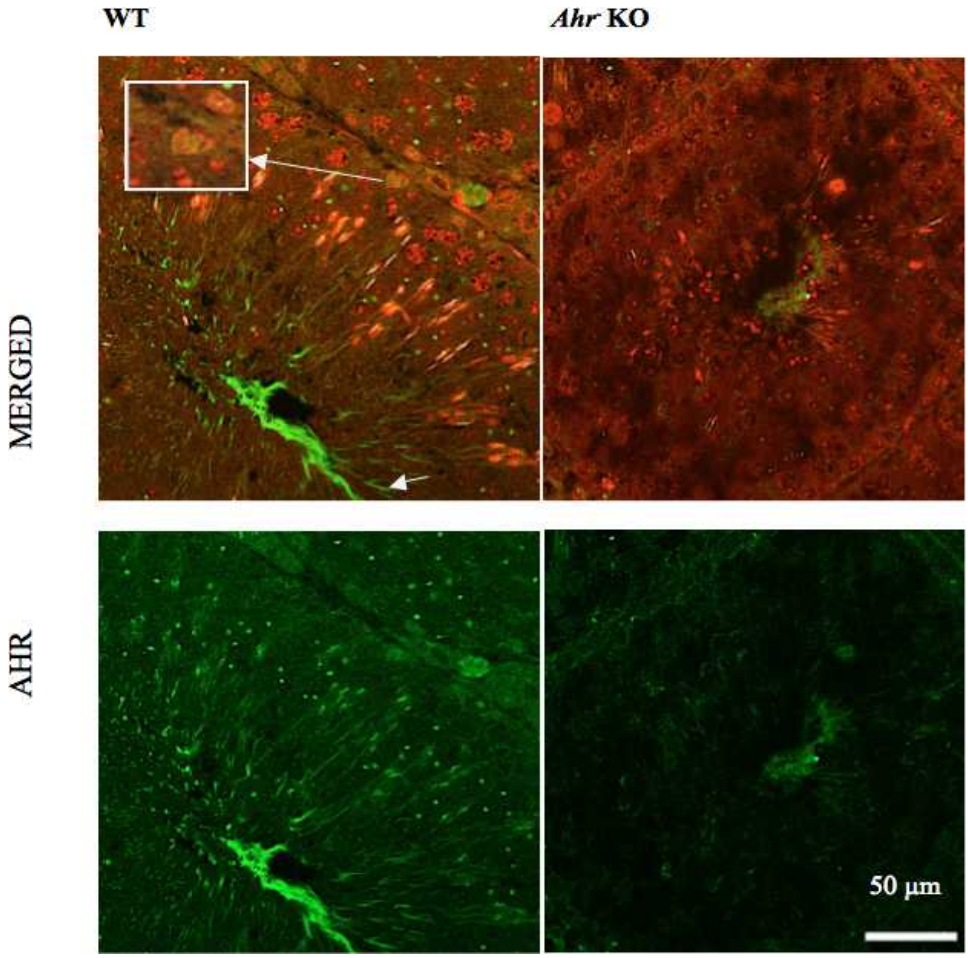

FIG. 10. Immunofluorescent localization of Ahr in testis. Seminiferous epithelia from WT and $Ahr^{-/-}$ (*Ahr*-KO) were probed with an AHR polyclonal antibody (green) and counterstained with Sytox (red). AHR-specific green fluorescence appears as granular staining in the cytoplasm of germ cells and as an intense signal on the luminal sperm. Arrow indicates filamentous staining. Arrow indicates the polygonal-shaped nucleus of a Sertoli cell. Leydig cells and peritubular myoid cells are present between the tubules. Bar = 50 µm.

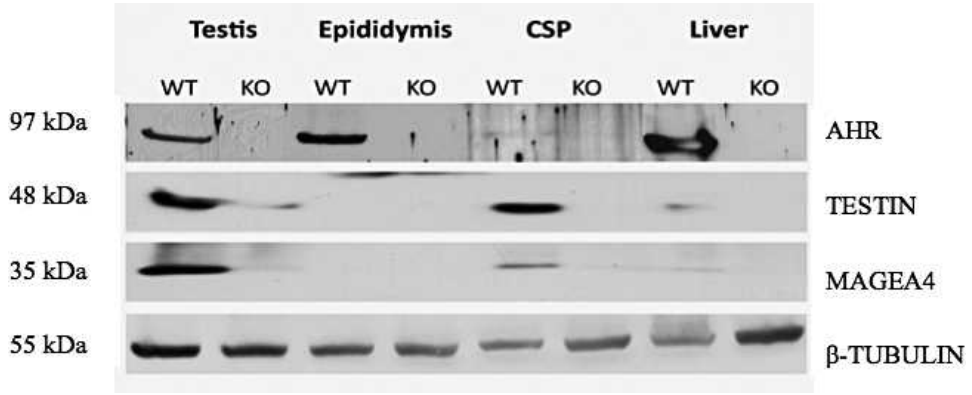

FIG. 11. Western blot analysis of AHR, TESTIN, and MAGEA4. Western blot analysis confirming AHR expression in the WT testis, epididymis, liver, and a faint signal in caudal sperm. The absence of AHR protein was confirmed in the $Ahr^{-/-}$ (KO) male, and TESTIN and MAGEA4 expression in the WT and $Ahr^{-/-}$ testes parallel the qRT-PCR data, with the virtual absence of these proteins in the $Ahr^{-/-}$ male. The presence of TESTIN and MAGEA4 in the WT caudal sperm requires further study. Sizes are indicated to the left. Beta-tubulin served as a loading control.

earlier studies noting no differences in the quantity of daily sperm production [23, 24], we also observed no differences in sperm quantity and motion parameters between $Ahr^{-/-}$ and WT mice. The relevance of these findings is uncertain given the high background rates of abnormal sperm in this study and in inbred strains [31]. Moreover, no standardized criteria exist for the evaluation of mouse sperm abnormalities such as the World Health Organization manual for human sperm analysis [55]. Nevertheless, when compared to WT, we found that $Ahr^{-/-}$ caudal sperm were less able to fertilize oocytes, indicating that AHR plays an important role in the development of fully functional sperm.

Our observations that loss of AHR results in decreased expression of genes involved in defense against reactive oxygen species (*Ucp2*, *Sod2*, and *Nrf2*) complement our previous results demonstrating that activation of AHR in spermatocytes leads to increased expression of these same family of genes [56]. In that study, cigarette smoke condensate (CSC), which contains numerous dioxin-like compounds, was used to activate AHR in spermatocytes. CSC treatment resulted in increased expression of *Sod2* and *Cyp1A1*. Similarly, spermatocytes isolated by laser microdissection from mice treated with CSC demonstrated increased expression of *Sod2,* the glutathione antioxidant *Gpx4,* and the antioxidant uncoupling protein *Ucp2* [56]. This body of work involving *Ahr* activation and now *Ahr* loss of function suggest that this signaling pathway may serve as a stress rheostat such that some degree of signaling is necessary for developmental homeostasis of male germ cells, however, overactivation leads to poor outcomes related to stress overload and an eventual inability to cope with excess stimulation. Further work in this area of reproductive toxicology will be necessary to discern the mechanisms responsible for the physiologic and pathologic roles that *Ahr* activation plays in male reproductive physiology.

ACKNOWLEDGMENT

The authors gratefully thank Dr. Deborah Frank for her suggestions and writing expertise.

REFERENCES

1. Thackaberry EA, Jiang Z, Johnson CD, Ramos KS, Walker MK. Toxicogenomic profile of 2,3,7,8-tetrachlorodibenzo-p-dioxin in the murine fetal heart: modulation of cell cycle and extracellular matrix genes. Toxicol Sci 2005; 88:231–241.
2. Barouki R, Coumoul X, Fernandez-Salguero PM. The aryl hydrocarbon receptor, more than a xenobiotic-interacting protein. FEBS Lett 2007; 581: 3608–3615.
3. Puga A, Marlowe J, Barnes S, Chang CY, Maier A, Tan Z, Kerzee JK, Chang X, Strobeck M, Knudsen ES. Role of the aryl hydrocarbon receptor in cell cycle regulation. Toxicology 2002; 181–182:171–177.
4. Grassman JA, Masten SA, Walker NJ, Lucier GW. Animal models of human response to dioxins. Environ Health Perspect 1998; 106(Suppl 2): 761–775.
5. National Research Council. Gulf War and Health: Volume 3. Fuels, Combustion Products, and Propellants. Washington, DC: The National Academies Press; 2005.
6. Fujiyoshi PT, Michalek JE, Matsumura F. Molecular epidemiologic evidence for diabetogenic effects of dioxin exposure in U.S. Air Force veterans of the Vietnam War. Environ Health Perspect 2006; 114: 1677–1683.
7. Roman BL, Pollenz RS, Peterson RE. Responsiveness of the adult male rat reproductive tract to 2,3,7,8-tetrachlorodibenzo-p-dioxin exposure: Ah receptor and ARNT expression, CYP1A1 induction, and Ah receptor down-regulation. Toxicol Appl Pharmacol 1998; 150:228–239.
8. Olshan AF, Teschke K, Baird PA. Birth defects among offspring of firemen. Am J Epidemiol 1990; 131:312–321.
9. Araneta MR, Schlangen KM, Edmonds LD, Destiche DA, Merz RD, Hobbs CA, Flood TJ, Harris JA, Krishnamurti D, Gray GC. Prevalence of birth defects among infants of Gulf War veterans in Arkansas, Arizona, California, Georgia, Hawaii, and Iowa, 1989–1993. Birth Defects Res A Clin Mol Teratol 2003; 67:246–260.
10. National Research Council. Veterans and Agent Orange: Update 2000. Washington, DC: The National Academies Press; 2001.
11. Deng K, Liu Z, Lin Y, Mu D, Chen X, Li J, Li N, Deng Y, Li X, Wang Y, Li S, Zhu J. Periconceptional paternal smoking and the risk of congenital heart defects: a case-control study. Birth Defects Res A Clin Mol Teratol 2013; 97:210–216.
12. Hammadeh ME, Hamad MF, Montenarh M, Fischer-Hammadeh C. Protamine contents and P1/P2 ratio in human spermatozoa from smokers and non-smokers. Hum Reprod 2010; 25:2708–2720.
13. Mukhopadhyay D, Nandi P, Varghese AC, Gutgutia R, Banerjee S, Bhattacharyya AK. The in vitro effect of benzo[a]pyrene on human sperm hyperactivation and acrosome reaction. Fertil Steril 2010; 94:595–598.
14. Mohamed el-SA, Song WH, Oh SA, Park YJ, You YA, Lee S, Choi JY, Kim YJ, Jo I, Pang MG. The transgenerational impact of benzo(a)pyrene on murine male fertility. Hum Reprod 2010; 25:2427–2433.
15. DiNatale BC, Murray IA, Schroeder JC, Flaveny CA, Lahoti TS, Laurenzana EM, Omiecinski CJ, Perdew GH. Kynurenic acid is a potent endogenous aryl hydrocarbon receptor ligand that synergistically induces interleukin-6 in the presence of inflammatory signaling. Toxicol Sci 2010; 115:89–97.
16. Jrad-Lamine A, Henry-Berger J, Gourbeyre P, Damon-Soubeyrand C, Lenoir A, Combaret L, Saez F, Kocer A, Tone S, Fuchs D, Zhu W, Oefner PJ, et al. Deficient tryptophan catabolism along the kynurenine pathway reveals that the epididymis is in a unique tolerogenic state. J Biol Chem 2011; 286:8030–8042.
17. Mezrich JD, Fechner JH, Zhang X, Johnson BP, Burlingham WJ, Bradfield CA. An interaction between kynurenine and the aryl

hydrocarbon receptor can generate regulatory T cells. J Immunol 2010; 185:3190–3198.
18. Aitken RJ, Roman SD. Antioxidant systems and oxidative stress in the testes. Oxid Med Cell Longev 2008; 1:15–24.
19. Matsumura F. The significance of the nongenomic pathway in mediating inflammatory signaling of the dioxin-activated Ah receptor to cause toxic effects. Biochem Pharmacol 2009; 77:608–626.
20. Gasiewicz T, Henry E. History of research in AHR. In: Pohjanvirta R (ed.), The AH Receptor in Biology and Toxicology. Hoboken, NJ: Wiley; 2012:3–32.
21. Schultz R, Suominen J, Varre T, Hakovirta H, Parvinen M, Toppari J, Pelto-Huikko M. Expression of aryl hydrocarbon receptor and aryl hydrocarbon receptor nuclear translocator messenger ribonucleic acids and proteins in rat and human testis. Endocrinology 2003; 144:767–776.
22. Karman B, Hernandez-Ochoa I, Ziv-Gal A, Flaws J. Involvement of the AHR in development and functioning of the female and male reproductive systems. In: Pohjanvirta R (ed.), The AH Receptor in Biology and Toxicology. Hoboken, NJ: Wiley; 2012:437–466.
23. Baba T, Shima Y, Owaki A, Mimura J, Oshima M, Fujii-Kuriyama Y, Morohashi KI. Disruption of aryl hydrocarbon receptor (AhR) induces regression of the seminal vesicle in aged male mice. Sex Dev 2008; 2: 1–11.
24. Lin TM, Ko K, Moore RW, Buchanan DL, Cooke PS, Peterson RE. Role of the aryl hydrocarbon receptor in the development of control and 2,3,7,8-tetrachlorodibenzo-p-dioxin-exposed male mice. J Toxicol Environ Health A 2001; 64:327–342.
25. Lee J, Richburg JH, Younkin SC, Boekelheide K. The Fas system is a key regulator of germ cell apoptosis in the testis. Endocrinology 1997; 138: 2081–2088.
26. Bustin SA, Benes V, Garson JA, Hellemans J, Huggett J, Kubista M, Mueller R, Nolan T, Pfaffl MW, Shipley GL, Vandesompele J, Wittwer CT. The MIQE guidelines: minimum information for publication of quantitative real-time PCR experiments. Clin Chem 2009; 55:611–622.
27. Guo R, Yu Z, Guan J, Ge Y, Ma J, Li S, Wang S, Xue S, Han D. Stage-specific and tissue-specific expression characteristics of differentially expressed genes during mouse spermatogenesis. Mol Reprod Dev 2004; 67:264–272.
28. Shima JE, McLean DJ, McCarrey JR, Griswold MD. The murine testicular transcriptome: characterizing gene expression in the testis during the progression of spermatogenesis. Biol Reprod 2004; 71:319–330.
29. Kent WJ, Sugnet CW, Furey TS, Roskin KM, Pringle TH, Zahler AM, Haussler D. The human genome browser at UCSC. Genome Res 2002; 12: 996–1006.
30. Swanson. Dioxin response elements and regulation of gene transcription. In: Pohjanvirta R (ed.) The AH Receptor in Biology and Toxicology. Hoboken, NJ: Wiley; 2012:81–87.
31. Kawai Y, Hata T, Suzuki O, Matsuda J. The relationship between sperm morphology and in vitro fertilization ability in mice. J Reprod Dev 2006; 52:561–568.
32. Perrault S, Klinefelter G, Clegg E. Assessment of male reproductive toxicology. In: Hayes AW (ed.), Principles and Methods of Toxicology, 5th ed. Boca Raton, FL: CRC Press; 2008:1605–1640.
33. O'Donnell L, Nicholls PK, O'Bryan MK, McLachlan RI, Stanton PG. Spermiation: the process of sperm release. Spermatogenesis 2011; 1: 14–35.
34. Sreedhar AS, Kalmar E, Csermely P, Shen YF. Hsp90 isoforms: functions, expression and clinical importance. FEBS Lett 2004; 562:11–15.
35. Mayer MP, Prodromou C, Frydman J. The Hsp90 mosaic: a picture emerges. Nat Struct Mol Biol 2009; 16:2–6.
36. Mammalian reproductive genetics. In: The Mammalian Reproductive Genetics Database. Seattle, WA: University of Washington. http://mrgd.org/index.cgi. Accessed 20 October 2013.
37. Seli E, Mahutte N, Arici A. The reproductive system from an immunologic perspective. Immunol Allergy Clinics N Am 2002; 22: 383–405.
38. Bhan S, Chuang A, Negi SS, Glazer CA, Califano JA. MAGEA4 induces growth in normal oral keratinocytes by inhibiting growth arrest and apoptosis. Oncol Rep 2012; 28:1498–1502.
39. Chomez P, De Backer O, Bertrand M, De Plaen E, Boon T, Lucas S. An overview of the MAGE gene family with the identification of all human members of the family. Cancer Res 2001; 61:5544–5551.
40. Esakky P, Hansen DA, Drury AM, Moley KH. Molecular analysis of cell type-specific gene expression profile during mouse spermatogenesis by laser microdissection and qRT-PCR. Reprod Sci 2013; 20:238–252.
41. He Z, Kokkinaki M, Jiang J, Dobrinski I, Dym M. Isolation, characterization, and culture of human spermatogonia. Biol Reprod 2010; 82:363–372.
42. Dietrich C. The AHR in control of cell cycle and apoptosis. In: Pohjanvirta R (ed.) The AH Receptor in Biology and Toxicology. Hoboken, NJ: Wiley; 2012:3–34.
43. Grima J, Wong CC, Zhu LJ, Zong SD, Cheng CY. Testin secreted by Sertoli cells is associated with the cell surface, and its expression correlates with the disruption of Sertoli-germ cell junctions but not the inter-Sertoli tight junction. J Biol Chem 1998; 273:21040–21053.
44. Cheng CK, Cheung CH, Lee WM. Mouse testin: complementary DNA cloning, genomic organization, and characterization of its proximal promoter region. Biol Reprod 2003; 68:1376–1386.
45. Eddy EM. Role of heat shock protein HSP70-2 in spermatogenesis. Rev Reprod 1999; 4:23–30.
46. Aitken RJ, De Iuliis GN. On the possible origins of DNA damage in human spermatozoa. Mol Hum Reprod 2010; 16:3–13.
47. Pi J, Bai Y, Daniel KW, Liu D, Lyght O, Edelstein D, Brownlee M, Corkey BE, Collins S. Persistent oxidative stress due to absence of uncoupling protein 2 associated with impaired pancreatic beta-cell function. Endocrinology 2009; 150:3040–3048.
48. Simmons SO, Fan CY, Ramabhadran R. Cellular stress response pathway system as a sentinel ensemble in toxicological screening. Toxicol Sci 2009; 111:202–225.
49. Sutovksy P, Manandhar G. Mammalian spermatogenesis and sperm structure. In: DeJonge C, Barrett C (eds.), The Sperm Cell: Production, Maturation, Fertilization and Regeneration. Cambridge, UK: Cambridge Press; 2006:1–30.
50. Boekelheide K. Mechanisms of toxic damage to spermatogenesis. J Natl Cancer Inst Monogr 2005; 6–8.
51. Lai KP, Wong MH, Wong CK. Effects of TCDD in modulating the expression of Sertoli cell secretory products and markers for cell-cell interaction. Toxicology 2005; 206:111–123.
52. Ma Q. Overview of AHR functional domains and the classical AHR signaling pathway: induction of drug metabolizing enzymes. In: Pohjanvirta R (ed.), The AH Receptor in Biology and Toxicology. Hoboken, NJ: Wiley; 2012:35–45.
53. Teo SK, Harden JL, Burke AB, Noormohamed FH, Youle M, Johnson MA, Peters BS, Stirling DI, Thomas SD. Thalidomide is distributed into human semen after oral dosing. Drug Metab Dispos 2001; 29:1355–1357.
54. National Research Council. Veterans and Agent Orange: Update 2012. Washington, DC: The National Academies Press; 2013.
55. Cooper TG, Noonan E, von Eckardstein S, Auger J, Baker HW, Behre HM, Haugen TB, Kruger T, Wang C, Mbizvo MT, Vogelsong KM. World Health Organization reference values for human semen characteristics. Hum Reprod Update 2010; 16:231–245.
56. Esakky P, Hansen DA, Drury AM, Moley KH. Cigarette smoke condensate induces aryl hydrocarbon receptor-dependent changes in gene expression in spermatocytes. Reprod Toxicol 2012; 34:665–676.